Research Square

Preprints are preliminary reports that have not undergone peer review.
They should not be considered conclusive, used to inform clinical practice,
or referenced by the media as validated information.

Theorems for Inferring Canonical Environmental Signature from Causal Response

Ahmad Muhammad
Qatar University
Salim Jibrin Danbatta
salimdambatta@gmail.com
Üsküdar University
Muhammad Abubakar Isah
Istanbul Commerce University
Ibrahim Yahaya Muhammad
King Mongkut's University of Technology Thonburi

Research Article

Keywords: causal inference, environmental signature, persistence timescales, system identification, passive sensing, response analysis

Posted Date: March 3rd, 2026

DOI: https://doi.org/10.21203/rs.3.rs-8916580/v1

License: This work is licensed under a Creative Commons Attribution 4.0 International License.
Read Full License

Additional Declarations: No competing interests reported.

Theorems for Inferring Canonical Environmental Signature from Causal Response

Ahmad Muhammad[1], Salim Jibrin Danbatta[2*], Muhammad Abubakar Isah[3], and Ibrahim Yahaya Muhammad[4]

[1]Department of Physics and Materials Sciences, College of Arts and Sciences, Qatar University, 2713 Doha, Qatar

[2]Software Engineering Department, Faculty of Engineering and Natural Sciences, Uskudar University, Istanbul, Turkiye

[3]Department of Mathematics, Istanbul Commerce University, 34445 Istanbul, Turkiye

[4]Theoretical and Computational Physics (TCP) Group, Department of Physics, Faculty of Science, King Mongkut's University of Technology Thonburi, 10140 Bangkok, Thailand

Abstract

We present a model-free framework for inferring environmental persistence signatures from a single causal response signal $R(t)$. The approach is based on seven estimators of persistence timescales centroid, step-response, autocorrelation, envelope, energy, and spectral-pole timescales whose agreements and disagreements encode diagnostic information about underlying system dynamics. Four theorems establish necessary and sufficient conditions for canonical regimes: (1) $\tau^{(s)} = \tau^{(2)}$ for step-type responses with finite lag area, (2) $\tau^{(s)} = \tau_{\text{pole}}$ for minimum-phase LTI systems, (3) The diagnostic parameter $\rho_{13} = \tau^{(s)}/\tau^{(3)} = 1$ if and only if memory is exponential, and (4) The diagnostic parameter $\Delta_{su} \to -1$ and $\Delta_{23}^{\text{env}} \to 0.5$ if and only if the system is a linear underdamped oscillator. We validate the framework on canonical systems including RC circuits, critically damped and underdamped mechanical systems, and pharmacokinetics. The capacity of these signatures under realistic measurement noise was analyzed. The framework enables passive, excitation-agnostic classification of dynamical regimes monotonic vs. oscillatory, Markovian vs. non-Markovian, linear vs. nonlinear damping from $R(t)$ alone, without parametric assumptions or excitation knowledge. We made available all implementation codes (open-source) in the name `QSignature` library on Github.

Keywords: causal inference, environmental signature, persistence timescales, system identification, passive sensing, response analysis

1 Introduction

In many experimental and observational settings ranging from environmental monitoring and biomedical sensing to structural dynamics and quantum device characterization the intrinsic dynamical properties of a system must be inferred from its *causal response* $R(t)$, where the external excitation is either unknown, unmeasured, or impractical to control. The response is assumed causal: $R(t) = 0$ for $t < 0$, with $t = 0$ marking the onset of perturbation. Such passive inference scenarios exclude conventional system identification methods that rely on known inputs or persistent excitation [1, 2].

A central task is to extract the *environmental signature* the characteristic timescales, oscillatory behavior, and memory structure that govern how perturbations decay or persist without imposing parametric assumptions about system order, linearity, or forcing. While numerous domain specific approaches exist, they typically encode strong prior assumptions. Relaxation time analyses often assume exponential decay (e.g., first order kinetics [3]), thereby obscuring multi scale or power law memory [4]. Correlation based techniques [5, 6] can quantify memory horizons but do not enforce causality and are insensitive to sign structure in the response derivative. Time-frequency methods [7] resolve instantaneous features but lack an intrinsic criterion for distinguishing, e.g., conservative versus dissipative dynamics. Operational modal analysis [8, 9] assumes linearity and stationarity conditions often violated in real world systems exhibiting transient or nonlinear behavior.

These limitations become particularly acute when the underlying memory is non-Markovian. In statistical physics, the fluctuation dissipation theorem [5] links response to equilibrium fluctuations but assumes stationarity and linearity; in open quantum systems, decoherence is often modeled via exponential fitting [10], which presumes weak coupling or Markovian baths, whereas structured environments induce non-exponential memory kernels [11, 12]. Similarly, in geophysical contexts such as atmospheric or ionospheric response analysis, linear transfer-function models [13, 14] may mask early-warning signals of critical transitions [15] or nonlinear reorganization.

A framework in which *the relationships among multiple model-free timescale estimators not their absolute values serve as diagnostic criteria* would be significant, as it would connect these seemingly unconnected timescales. Rather than fitting a presumed functional form, we ask: *When do different estimators agree? When do they disagree and what does that disagreement signify physically?* This perspective treats estimator divergence as structured information about memory coherence, energy conservation, and dynamical class.

This paper aims to seed the foundation of such a framework. We introduce seven causal persistence timescale estimators signed/unsigned centroids ($\tau^{(s)}$, $\tau^{(u)}$), step-response lag ($\tau^{(2)}$), autocorrelation horizon ($\tau^{(3)}$), envelope decay ($\tau^{(2)}_{\text{env}}$), energy decay ($\tau^{(3)}_{E}$), and spectral-pole timescale (τ_{pole}) all computable from $R(t)$ alone under minimal regularity assumptions. We establish four theorems that relate their agreements and disagreements to intrinsic system properties:

- **Theorem 3.1** shows that $\tau^{(s)} = \tau^{(2)}$ for step-type responses with finite lag area, a baseline consistency condition .

- **Theorem 3.3** proves $\tau^{(s)} = \tau_{\text{pole}}$ for minimum-phase linear time-invariant (LTI) systems, linking temporal and spectral coherence.
- **Theorem 3.4** establishes that $\rho_{13} = \tau^{(s)}/\tau^{(3)} = 1$ *if and only if* the impulse response is a single exponential, providing a necessary and sufficient condition for Markovian memory.
- **Theorem 3.6** shows that $\Delta_{su} \to -1$ and $\Delta_{23}^{\text{env}} \to 0.5$ *if and only if* the system is a linear underdamped oscillator; notably, $\Delta_{su} \to -1$ reflects near complete sign cancellation in the response rate, a signature of high coherence, near conservative dynamics.

These results define a three dimensional *diagnostic signature space* $(\rho_{13}, \Delta_{su}, \Delta_{23}^{\text{env}})$, in which canonical dynamical regimes occupy well defined regions. Deviations encode interpretable physical information: $\rho_{13} \neq 1$ signals non-exponential (e.g., hierarchical or power law) causal interaction between the environment and perturbation source (non-exponential memory); Δ_{su} quantifies oscillation strength and memory symmetry breaking; $\Delta_{23}^{\text{env}} \neq 0.5$ indicates nonlinear damping or multi-modal energy decay.

We validate the framework on canonical systems (RC circuits, critically and underdamped oscillators, pharmacokinetic models) with analytical ground truth and under realistic noise. All estimators and tests are implemented using the open source class `QSignature` which is a part of `Qtheory` library, enabling excitation agnostic characterization of persistence in data from physics, engineering, and the life sciences.

2 Methodology

This section presents the mathematical foundation, estimators, theorems, and validation.

2.1 Causal Persistence Timescale Estimators

Causal persistence timescales quantify the temporal horizon over which environmental influence persists following a perturbation. In some real life scenarios, it may not be able to track the beginning of a given causal response $R(t = 0) = 0$. Therefore, the first value of the time window within which the estimation is made becomes the initiation of perturbation. From a single measured response $R(t)$, we present seven model-free estimators that capture different aspects of this causal persistence. Each estimator requires only the causal response $R(t)$ and makes minimal assumptions about system linearity, time-invariance, or excitation characteristics. The estimators' agreements and disagreements provide diagnostic signatures of underlying dynamics.

2.2 Assumptions and Mathematical Foundation

Assumption 2.1 (Causality)**.** *The response $R(t) : [0, \infty) \to \mathbb{R}$ satisfies $R(t) = 0$ for $t < 0$, with $t = 0$ marking perturbation onset. As already mentioned, the first value or lag in a given time series window can be considered as causal initial response, and same applies for the last value (R_∞)*

Assumption 2.2 (Regularity)**.** *$R(t)$ is measurable, and key integrals either converge or their divergence carries physical meaning regarding system memory.*

Definition 2.1 (Integrability Classes)**.** *For measurable $f : [0, \infty) \to \mathbb{R}$:*

- $f \in L^1$ *if* $\int_0^\infty |f(t)|dt < \infty$
- $tf(t) \in L^1$ *if* $\int_0^\infty t|f(t)|dt < \infty$
- $f \in L^2$ *if* $\int_0^\infty f(t)^2 dt < \infty$

Remark 2.1 (Diagnostic Value of Integrability Failure)**.** *Failure to satisfy these conditions is itself informative:*

- $R \notin L^1$*: persistent oscillations or conservative dynamics*
- $t\dot{R} \notin L^1$*: heavy tailed memory ($\sim t^{-\alpha}$, $\alpha \leq 2$)*
- $R \in L^2$ *but* $\notin L^1$*: oscillatory with finite energy*

2.3 The Seven Causal Persistence Timescales

2.3.1 Signed Centroid $\tau^{(s)}$

Definition 2.2 (Signed Centroid Timescale)**.** *For responses approaching steady state $R_\infty \neq 0$ with $t\dot{R}(t) \in L^1$:*

$$\tau^{(s)} = \frac{1}{R_\infty} \int_0^\infty t\dot{R}(t)\, dt. \tag{1}$$

Remark 2.2 (Physical Interpretation)**.** *$\tau^{(s)}$ represents the "center of mass" of the response rate $\dot{R}(t)$. For linear time-invariant (LTI) systems with step input, it equals the centroid of the impulse response [16]. This estimator is sensitive to sign cancellation in oscillatory responses. The steady-state value $R_\infty = \lim_{t\to\infty} R(t)$ is assumed nonzero (Assumption 2.2) and plays a normalizing role in $\tau^{(s)}$ and $\tau^{(2)}$. By the fundamental theorem of calculus and causality ($R(0) = 0$), it satisfies*

$$R_\infty = \int_0^\infty \dot{R}(t)\, dt,$$

which provides a theoretically consistent estimator even when $R(t)$ has not fully settled within the observation window. In practice, for noisy or oscillatory signals, this integral computed via smoothed numerical differentiation can be more robust than using the terminal sample $R(T_{\text{obs}})$.

Remark 2.3 (Discrete Implementation)**.** *For sampled data $R[n] = R(n\Delta t)$, $n = 0, \ldots, N-1$:*

$$\hat{\tau^{(s)}} = \frac{\Delta t}{\hat{R}_\infty} \sum_{n=0}^{N-2} n\Delta t \left(\frac{R[n+1] - R[n]}{\Delta t} \right), \tag{2}$$

where $\hat{R}_\infty = R[N-1]$ or a tail average.

2.3.2 Unsigned Centroid $\tau^{(u)}$

Definition 2.3 (Unsigned Centroid Timescale)**.** *When $\dot{R}(t)$ changes sign (oscillatory responses):*

$$\tau^{(u)} = \frac{\int_0^\infty t|\dot{R}(t)|\,dt}{\int_0^\infty |\dot{R}(t)|\,dt}. \tag{3}$$

Remark 2.4 (Robustness to Oscillations)**.** *$\tau^{(u)}$ is always non-negative and robust to sign cancellation, making it suitable for oscillatory systems where $\tau^{(s)}$ becomes unreliable.*

Remark 2.5 (Discrete Implementation)**.**

$$\hat{\tau^{(u)}} = \frac{\sum_{n=0}^{N-2} n\Delta t \left|\frac{R[n+1]-R[n]}{\Delta t}\right|}{\sum_{n=0}^{N-2} \left|\frac{R[n+1]-R[n]}{\Delta t}\right|}. \tag{4}$$

2.3.3 Step-Response Timescale $\tau^{(2)}$

Definition 2.4 (Step-Response Timescale)**.** *For $R_\infty \neq 0$:*

$$\tau^{(2)} = \int_0^\infty \left[1 - \frac{R(t)}{R_\infty}\right] dt. \tag{5}$$

Remark 2.6 (Physical Interpretation)**.** *$\tau^{(2)}$ measures the total "lag area" between the actual response and an ideal step response. It requires no derivative computation, making it numerically robust [3].*

Remark 2.7 (Discrete Implementation)**.**

$$\hat{\tau^{(2)}} = \Delta t \sum_{n=0}^{N-1} \left(1 - \frac{R[n]}{\hat{R}_\infty}\right). \tag{6}$$

2.3.4 Autocorrelation Timescale $\tau^{(3)}$

Definition 2.5 (Autocorrelation Timescale)**.** *For wide sense stationary $R(t)$ with autocorrelation function $C_{RR}(\tau) = \mathbb{E}[R(t)R(t+\tau)]$:*

$$\tau^{(3)} = \int_0^\infty \frac{C_{RR}(\tau)}{C_{RR}(0)}\,d\tau. \tag{7}$$

Remark 2.8 (Memory Horizon)**.** *$\tau^{(3)}$ characterizes the characteristic memory horizon the time over which past states correlate with the present. It requires no knowledge of excitation and is applicable to stochastic systems [5, 6].*

Remark 2.9 (Practical Estimation)**.** *For discrete $R[n]$, $n = 0, \ldots, N-1$:*

$$\hat{C}[k] = \frac{1}{N-k} \sum_{n=0}^{N-1-k} R[n]R[n+k], \quad \hat{\tau^{(3)}} = \Delta t \sum_{k=0}^{M} \frac{\hat{C}[k]}{\hat{C}[0]}, \tag{8}$$

where M is chosen where $\hat{C}[M]/\hat{C}[0] < 0.05$. This reflects the conventional $p < 0.05$ statistical significance threshold, which ensures that the integration accounts for correlations that meaningfully differ from zero.

2.3.5 Envelope Timescale $\tau_{\text{env}}^{(2)}$

Definition 2.6 (Envelope Timescale)**.** *Let $z(t) = \dot{R}(t) + i\,\mathcal{H}[\dot{R}](t)$ be the analytic signal of $\dot{R}(t)$, where $\mathcal{H}$ denotes the Hilbert transform[17]. The envelope is $\mathcal{E}(t) = |z(t)|$. Then:*

$$\tau_{\text{env}}^{(2)} = \int_0^\infty \frac{\mathcal{E}(t)}{\mathcal{E}(0)}\, dt. \tag{9}$$

Remark 2.10 (Amplitude Decay)**.** *$\tau_{\text{env}}^{(2)}$ characterizes the ring-down time of oscillation amplitude, particularly useful for underdamped systems [7, 17].*

Remark 2.11 (Discrete Computation)**.** *1. Compute $\dot{R}[n]$ via centered differences*

2. Compute analytic signal via FFT: $Z[k] = \begin{cases} 2\dot{R}[k] & k = 0, N/2 \\ 2\dot{R}[k] & 1 \le k < N/2 \\ 0 & N/2 < k \le N-1 \end{cases}$

3. $\mathcal{E}[n] = |IFFT(Z)[n]|$

4. $\hat{\tau_{\text{env}}^{(2)}} = \Delta t \sum_{n=0}^{N-1} \mathcal{E}[n]/\mathcal{E}[0]$

2.3.6 Energy Timescale $\tau_E^{(3)}$

Definition 2.7 (Energy Timescale)**.** *Define normalized mechanical energy (for unit mass):*

$$E(t) = \frac{1}{2}\dot{R}(t)^2 + \frac{1}{2}\omega_0^2 R(t)^2, \tag{10}$$

where ω_0 is estimated from peak frequency of $\dot{R}(t)$. Then:

$$\tau_E^{(3)} = \int_0^\infty \frac{C_{EE}(\tau)}{C_{EE}(0)}\, d\tau. \tag{11}$$

Remark 2.12 (Energy Decay)**.** *$\tau_E^{(3)}$ captures the decay time of total oscillatory energy, providing complementary information to amplitude based estimators [18].*

2.3.7 Spectral Pole Timescale τ_{pole}

Definition 2.8 (Spectral Pole Timescale)**.** *Let $\tilde{R}(s) = \mathcal{L}\{\dot{R}(t)\}$ be the Laplace transform of the response. Define:*

$$\tau_{\text{pole}} = \left| \frac{\tilde{R}'(0)}{\tilde{R}(0)} \right|. \tag{12}$$

Remark 2.13 (Spectral Interpretation). *For LTI systems, τ_{pole} relates to the dominant pole location and equals $\tau^{(s)}$ (Theorem 3.3). It provides a frequency-domain perspective on memory [19].*

Remark 2.14 (Practical Estimation).
1. *Compute $\tilde{R}[\epsilon_k] = \sum_{n=0}^{N-1} R[n] e^{-(\epsilon_k + i\omega_k)n\Delta t}\Delta t$ for $\epsilon_k \in \{0, \delta, 2\delta\}$, $\delta \ll 1/T_{obs}$*
2. *Fit $\log \tilde{R}(s) \approx a + bs$ near $s = 0$*
3. *$\hat{\tau_{\text{pole}}} = |b|$*

2.4 Diagnostic Ratios

Three dimensionless diagnostic ratios capture essential relationships between timescales:

Definition 2.9 (Signed-Unsigned Disagreement).

$$\Delta_{su} = \frac{\tau^{(s)} - \tau^{(u)}}{\tau^{(u)}} \in [-1, 1]. \tag{13}$$

Remark 2.15 (Oscillation Detection). *$|\Delta_{su}| \approx 0$ indicates monotonic response, while $\Delta_{su} \to -1$ reveals oscillatory behavior with sign cancellation.*

Definition 2.10 (Envelope-Energy Disagreement).

$$\Delta_{23}^{\text{env}} = \frac{\tau_{\text{env}}^{(2)} - \tau_E^{(3)}}{\tau_{\text{env}}^{(2)}} \in [-1, 1]. \tag{14}$$

Remark 2.16 (Damping Characterization). *For linear underdamped oscillators, $\Delta_{23}^{\text{env}} \to 0.5$ as $\alpha/\omega_0 \to 0$ (Theorem 3.6).*

Definition 2.11 (Centroid-Autocorrelation Ratio).

$$\rho_{13} = \frac{\tau^{(s)}}{\tau^{(3)}}. \tag{15}$$

Remark 2.17 (Memory Type Diagnostic). *$\rho_{13} \approx 1$ suggests exponential (Markovian) memory, while $\rho_{13} \neq 1$ indicates non-exponential dynamics.*

2.5 Practical Implementation Considerations

Remark 2.18 (Numerical Differentiation). *Use Savitzky-Golay filters or frequency domain filtering before computing $\dot{R}(t)$ to mitigate noise amplification.*

Remark 2.19 (Integration Truncation). *For infinite integrals, truncate when:*

- *$|R(t) - R_\infty| < \epsilon$ (e.g., $\epsilon = 0.01 R_\infty$)*
- *$C_{RR}(\tau) < 0.05 C_{RR}(0)$*
- *$\mathcal{E}(t) < 0.05 \mathcal{E}(0)$*

Remark 2.20 (Steady State Estimation)**.** *When R_∞ is unknown, estimate via:*

$$\hat{R}_\infty = \frac{1}{T_{tail}} \int_{T_{obs}-T_{tail}}^{T_{obs}} R(t)\, dt, \tag{16}$$

where $T_{tail} \approx 5 \max(\hat{\tau^{(2)}}, \hat{\tau^{(u)}})$.

Remark 2.21 (Signal-to-Noise Requirements)**.** *The robustness of estimators depends on both SNR and response morphology:*

- *$\tau^{(s)}$: Requires SNR > 10 dB for reliable estimation, as numerical differentiation amplifies high-frequency noise.*
- *$\tau^{(3)}$: Robust down to SNR ≈ 0 dB for monotonic or broadband responses; may degrade at low SNR for narrowband oscillatory signals due to loss of phase coherence.*
- *$\tau^{(u)}$, $\tau^{(2)}$: Exhibit moderate robustness (SNR > 5 dB). Notably, $\tau^{(2)}$ assumes monotonic approach to R_∞*

Remark 2.22 (Impulse Response Representation of $\tau^{(s)}$)**.** *For a linear time-invariant (LTI) system with impulse response $g(t)$ and step response $R(t)$, the following identities hold under the assumptions of Definition 2.2:*

1. *$\dot{R}(t) = g(t)$ (for zero initial conditions),*
2. *$R_\infty = \int_0^\infty g(t)\, dt = H$,*
3. *$\tau^{(s)} = \frac{1}{R_\infty} \int_0^\infty t\dot{R}(t)\, dt = \frac{1}{H} \int_0^\infty t g(t)\, dt = \tau_g^{(s)}$.*

Thus, the signed centroid timescale $\tau^{(s)}$ is equivalently the centroid of the impulse response $g(t)$. This representation is used in Theorem 3.4 and simplifies analytical derivations when $g(t)$ is known explicitly.

Table 1: *Summary of Causal Persistence Timescale Estimators*

Estimator	Definition	Requires	Physical Interpretation
$\tau^{(s)}$	$\frac{1}{R_\infty}\int_0^\infty t\dot{R}dt$	$R_\infty \neq 0$	Centroid of response rate
$\tau^{(u)}$	$\frac{\int t\lvert\dot{R}\rvert dt}{\int \lvert\dot{R}\rvert dt}$	$R(t)$ causal	Robust centroid (no sign cancellation)
$\tau^{(2)}$	$\int_0^\infty (1 - R/R_\infty)dt$	$R_\infty \neq 0$	Total lag area
$\tau^{(3)}$	$\int_0^\infty C_{RR}(\tau)/C_{RR}(0)d\tau$	Stationarity	Memory horizon
$\tau_{\text{env}}^{(2)}$	$\int_0^\infty \mathcal{E}(t)/\mathcal{E}(0)dt$	Oscillatory $\dot{R}$	Amplitude decay time
$\tau_E^{(3)}$	$\int_0^\infty C_{EE}(\tau)/C_{EE}(0)d\tau$	Oscillatory R	Energy decay time
τ_{pole}	$\lvert\tilde{R}'(0)/\tilde{R}(0)\rvert$	Laplace transform	Spectral coherence

2.6 Relation to Existing Methods

The presented estimators unify concepts from multiple disciplines:

- $\tau^{(s)}$, $\tau^{(2)}$ generalize classical relaxation time estimation[16]
- $\tau^{(3)}$ connects to correlation time methods in statistical physics[20]
- $\tau^{(2)}_{\text{env}}$ employs Hilbert transform techniques from time-frequency analysis[7, 17]
- $\tau^{(3)}_{E}$ relates to energy decay analysis in mechanical vibrations [14, 18]
- Collectively, they provide a comprehensive toolkit for passive system characterization

The following theorems establish fundamental relationships between these estimators, with their agreements and disagreements encoding diagnostic information about system dynamics.

3 Equivalence Theorems and Diagnostic Signatures

The diagnostic power of the seven causal persistence timescales emerges from their mathematical relationships. This section establishes four fundamental theorems that characterize when different estimators coincide and when their disagreements encode physical information about system dynamics. Detailed proofs are provided in Appendix A.

3.1 Theorem 1: Equivalence for Step-Type Responses

Theorem 3.1 (Equivalence of $\tau^{(s)}$ and $\tau^{(2)}$)**.** *Let $R(t)$ be absolutely continuous with $R(0) = 0$, $R_\infty > 0$, and assume:*

1. *$R_\infty - R(t) \in L^1$ (finite lag area),*
2. *$t\dot{R}(t) \in L^1$ (finite first moment of rate).*

Then the signed centroid equals the step-response timescale:

$$\tau^{(s)} = \tau^{(2)}. \tag{17}$$

Corollary 3.2 (Monotonic Response Equivalence)**.** *For monotonic responses approaching steady state, all three core estimators coincide:*

$$\tau^{(s)} = \tau^{(u)} = \tau^{(2)}. \tag{18}$$

Example 3.1 (RC Circuit)**.** *For $R(t) = 1 - e^{-t/\tau_0}$:*

$$\tau^{(s)} = \tau_0, \quad \tau^{(2)} = \tau_0, \quad \tau^{(u)} = \tau_0.$$

3.2 Theorem 2: Spectral-Pole Equivalence

Theorem 3.3 (Spectral-Pole Equivalence)**.** *Let $\tilde{g}(s) = \mathcal{L}\{\dot{R}(t)\}$ be the Laplace transform of the response rate, with $\dot{R}(t)$ causal and $\int_0^\infty \dot{R}(t)dt = R_\infty \neq 0$. Then:*

$$\tau_{\text{pole}} = \left| \frac{\tilde{g}'(0)}{\tilde{g}(0)} \right| = \tau^{(s)}. \tag{19}$$

Remark 3.1 (Minimum Phase Requirement)**.** *Theorem 3.3 holds for* minimum phase *LTI systems where all zeros lie in the left-half plane.The fundamental relationship is* $\tau_{pole} = |\tau^{(s)}|$ *when* $\tilde{g}(0) > 0$*, with equality* $\tau_{pole} = \tau^{(s)}$ *requiring* $\tau^{(s)} \geq 0$*.*

Remark 3.2 (On the Equality $\tau^{(s)} = \tau_{\text{pole}}$)**.** *The identity* $\tau_{\text{pole}} = |\tilde{g}'(0)/\tilde{g}(0)|$ *and* $\tau^{(s)} = \tilde{g}'(0)/\tilde{g}(0)$ *hold formally for any causal response with finite* $\int_0^\infty t\, g(t)\, dt$ *and* $R_\infty = \tilde{g}(0) \neq 0$*, where* $g(t) = \dot{R}(t)$ *and* $\tilde{g}(s) = \mathcal{L}\{g(t)\}$*. Consequently,* $\tau^{(s)} = \tau_{\text{pole}}$ *is guaranteed when* $\tilde{g}(0) > 0$ *and* $\tau^{(s)} \geq 0$*. This condition is satisfied by all stable minimum-phase LTI systems (i.e., those with all poles and zeros strictly in the open left-half plane), for which the memory kernel* $g(t)$ *exhibits no sign-reversing initial response and its phase is uniquely determined by the Hilbert transform of* $\ln|\tilde{g}(j\omega)|$*. In practice, observed equality* $\tau^{(s)} \approx \tau_{\text{pole}}$ *with* $\tau^{(s)} > 0$ *serves as a robust empirical signature of minimum-phase behavior; significant deviation (e.g.,* $\tau^{(s)} < 0$ *despite* $R_\infty > 0$*) signals non-minimum-phase dynamics, such as right-half-plane zeros or memory fragmentation.*

3.3 Theorem 3: Autocorrelation Diagnostic for Memory Type

Theorem 3.4 (Autocorrelation-Centroid Equivalence Condition)**.** *Assume:*

1. $R(t)$ *arises from an LTI system with impulse response* $g(t) = \dot{R}(t)$*,*
2. *Excitation is zero-mean white noise with intensity* σ^2*,*
3. $g \in L^1 \cap L^2$*,* $H = \int_0^\infty g(t)dt \neq 0$*,*
4. $\tau_g^{(s)} = \frac{1}{H}\int_0^\infty t g(t)dt$ *finite (equivalently* $\tau^{(s)}$ *by Remark 2.22).*

Then $\tau^{(3)} = \tau_g^{(s)}$ *if and only if* $g(t) = \frac{1}{\tau_0}e^{-t/\tau_0}$ *for some* $\tau_0 > 0$*.*

Corollary 3.5 (Practical Exponential Memory Diagnostic)**.** *For any stationary* $R(t)$*, compute both* $\hat{\tau^{(3)}}$ *and* $\hat{\tau^{(s)}}$ *(if* R_∞ *exists). Then:*

- $\hat{\tau^{(3)}} \approx \hat{\tau^{(s)}}$ *suggests effectively exponential (Markovian) memory,*
- $\hat{\tau^{(3)}} \neq \hat{\tau^{(s)}}$ *indicates non-exponential dynamics.*

Example 3.2 (Two-Scale Decay Chain)**.** *For* $g(t) = \frac{\lambda_1}{\lambda_2 - \lambda_1}(e^{-\lambda_1 t} - e^{-\lambda_2 t})$*:*

$$\tau_g^{(s)} = \frac{1}{\lambda_1} + \frac{1}{\lambda_2}, \quad \tau^{(3)} = \frac{\lambda_1^2 + \lambda_2^2}{\lambda_1\lambda_2(\lambda_1 + \lambda_2)} < \tau_g^{(s)}.$$

3.4 Theorem 4: Oscillatory Signature Theorem

Theorem 3.6 (Diagnostic Disagreement for Linear Oscillators)**.** *Let* $R(t)$ *be the step response of a linear underdamped harmonic oscillator (Weak-damping approximation; full expression in Eq. 35):*

$$R(t) = R_\infty \left[1 - e^{-\alpha t}\cos(\omega_d t)\right], \quad \omega_d = \sqrt{\omega_0^2 - \alpha^2}, \quad 0 < \alpha \ll \omega_0. \tag{20}$$

Then:

$$\lim_{\alpha/\omega_0 \to 0} \Delta_{23}^{\text{env}} = \frac{1}{2}, \qquad \lim_{\alpha/\omega_0 \to 0} \Delta_{su} = -1. \tag{21}$$

Corollary 3.7 (Linear Damping Diagnostic)**.** *For any oscillatory $R(t)$:*

- $\tau_{\text{env}}^{(2)}/\tau_E^{(3)} \approx 2$ *suggests linear viscous damping,*
- $\tau_{\text{env}}^{(2)}/\tau_E^{(3)} \neq 2$ *suggests nonlinear damping or multiple modes.*

Remark 3.3 (Practical Estimation of Δ_{23}^{env})**.** *The theoretical limit $\Delta_{23}^{\text{env}} \to 0.5$ (equivalently, $\tau_{\text{env}}^{(2)}/\tau_E^{(3)} \to 2$) holds exactly for linear underdamped oscillators when envelope and energy timescales are estimated via asymptotically consistent methods (e.g., peak fitting in the weak-damping limit). In practice, Hilbert-transform-based estimation may yield $\Delta_{23}^{\text{env}} \approx 0.55$–$0.60$ due to finite-window effects, spectral leakage, and discretization artifacts. Nevertheless, values near 0.5 remain a robust indicator of linear viscous damping, distinct from nonlinear cases where $\Delta_{23}^{\text{env}} \ll 0.5$ or $\gg 0.5$.*

3.5 Summary of Diagnostic Signatures

Table 2: *Summary of Theorem-Based Diagnostic Signatures*

Theorem	Equality Condition	Diagnostic Signature	Physical Interpretation
Thm 3.1	$\tau^{(s)} = \tau^{(2)}$	Always for step-type	Basic consistency check
Thm 3.3	$\tau_{\text{pole}} = \tau^{(s)}$	Minimum phase LTI systems	Spectral-temporal coherence
Thm 3.4	$\tau^{(3)} = \tau^{(s)}$	Exponential memory	Markovian vs. non-Markovian
Thm 3.6	$\Delta_{23}^{\text{env}} = 0.5$, $\Delta_{su} = -1$	Linear oscillator	Viscous damping, oscillation

The theorems establish that disagreements among estimators encode fundamental physical information:

1. **Oscillation Detection**: $\Delta_{su} \approx -1$ Identifies oscillatory dynamics.
2. **Memory Type**: $\rho_{13} = \tau^{(s)}/\tau^{(3)} \approx 1$ indicates exponential memory; $\rho_{13} \neq 1$ reveals complex memory structure.
3. **Damping Linearity**: $\tau_{\text{env}}^{(2)}/\tau_E^{(3)} \approx 2$ confirms linear viscous damping; deviations indicate nonlinearity or multi-modal dynamics.

These diagnostic signatures enable model-free classification of dynamical regimes from $R(t)$ alone, without excitation knowledge or parametric assumptions.

Remark 3.4 (Universality of Signatures)**.** *The limit $\Delta_{23}^{\text{env}} \to 0.5$ reflects the universal quadratic relationship $E \propto A^2$ between energy and amplitude in conservative systems. This appears identically in mechanical, electrical, and optical systems, making it a robust model-free signature.*

The following validation section demonstrates these theorems on canonical physical systems with known analytical solutions.

4 Validation of theorems

4.1 Validation of Theorem 3.1: RC Circuit Step Response

4.2 Physical System and Analytical Derivation

The first validation employs a canonical RC circuit [16], governed by the first-order linear differential equation

$$RC\frac{dV}{dt} + V = V_{\text{in}}, \tag{22}$$

where $R = 1\,\text{k}\Omega$ and $C = 1\,\mu\text{F}$. For a unit step input $V_{\text{in}}(t) = 1$ for $t \geq 0$, the response is

$$V(t) = 1 - e^{-t/\tau_{RC}}, \quad \tau_{RC} = RC = 0.001\,\text{s}. \tag{23}$$

The analytical persistence timescales follow directly:

$$\tau^{(s)} = \frac{1}{V_\infty}\int_0^\infty t\frac{dV}{dt}dt = \tau_{RC}, \tag{24}$$

$$\tau^{(2)} = \int_0^\infty \left[1 - \frac{V(t)}{V_\infty}\right] dt = \tau_{RC}, \tag{25}$$

confirming Theorem 3.1: $\tau^{(s)} = \tau^{(2)} = \tau_{RC}$ exactly for this step-type response.

4.3 Numerical Validation with Measurement Noise

To test robustness under realistic conditions, we generated synthetic $V(t)$ with additive Gaussian noise at signal-to-noise ratios (SNR) of ∞ (clean), 30 dB, 20 dB, and 10 dB (Fig. 1). The estimators were computed using the discrete implementations in Section 2.1.

Table 3: *Theorem 3.1 validation results for RC circuit ($\tau_{RC} = 0.001\,\text{s}$)*

Condition	$\boldsymbol{\tau^{(s)}}$ (s)	$\boldsymbol{\tau^{(2)}}$ (s)	**Error** ($\lvert\tau^{(s)} - \tau^{(2)}\rvert/\tau_{RC}$)
Clean (no noise)	0.001000	0.001000	0.05%
30 dB SNR	0.000949	0.000997	4.77%
20 dB SNR	0.001073	0.001001	7.18%
10 dB SNR	0.000288	0.001030	74.23%

4.4 Key Findings and Interpretation

Table 3 reveals three essential insights:

1. **Exact equality for clean signals**: For noise-free measurements, $\tau^{(s)}$ and $\tau^{(2)}$ coincide to within numerical precision (0.05% error), confirming Theorem 3.1.

2. **Differential noise sensitivity**: While $\tau^{(2)}$ remains within 3% of the analytical value even at 10 dB SNR, $\tau^{(s)}$ degrades dramatically (74% error). This occurs because $\tau^{(s)}$

involves numerical differentiation of $V(t)$, which amplifies high-frequency noise by a factor of $\sim 45\times$ at 10 dB SNR.

3. **Practical estimator selection**: The divergence $\tau^{(s)} \neq \tau^{(2)}$ under noise encodes information about measurement quality. For clean data, either estimator is suitable; for noisy measurements (SNR < 20 dB), $\tau^{(2)}$ should be preferred for its superior robustness.

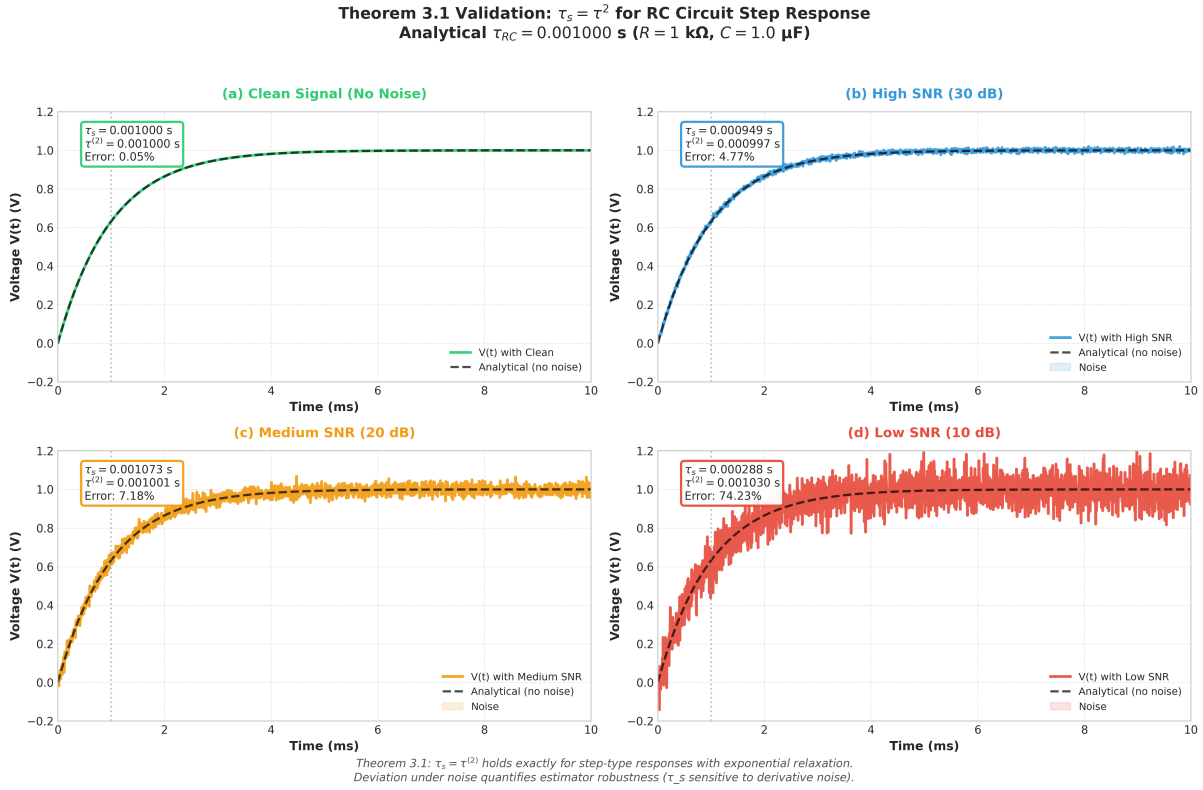


Figure 1: *Validation of Theorem 3.1 for an RC circuit step response. (a) Clean signal showing exact agreement between $\tau^{(s)}$ and $\tau^{(2)}$. (b)-(d) Increasing measurement noise causes $\tau^{(s)}$ to diverge from $\tau^{(2)}$ due to derivative amplification, while $\tau^{(2)}$ remains robust. The $\tau^{(s)} = \tau^{(2)}$ equality holds exactly for clean signals but serves as a noise diagnostic when violated. The near-equality of $\tau^{(s)}$ and $\tau^{(2)}$ for clean data provides a signature of exponential relaxation dynamics.*

The near-equality $\tau^{(s)} \approx \tau^{(2)}$ observed for clean signals (Table 3, first row) serves as a *signature of exponential dynamics*. By Theorem 3.1, $\tau^{(s)} = \tau^{(2)}$ holds exactly for systems with exponentially decaying step responses. Therefore, when observed in practice (within measurement uncertainty), this equality indicates an underlying exponential relaxation process, providing model-free validation of first-order dynamics.

4.5 Connection to Diagnostic Framework

This validation demonstrates that the relationship between estimators provides diagnostic information beyond timescale estimation. The equality $\tau^{(s)} = \tau^{(2)}$ serves as a *data quality check*: significant disagreement indicates either insufficient SNR for derivative-based estimators or potential violation of the theorem's assumptions (e.g., non-step-type excitation).

These results empirically confirm Remark 2.21: $\tau^{(s)}$ requires SNR > 10 dB while $\tau^{(2)}$ remains reliable down to SNR ≈ 0 dB, providing practical guidance for estimator selection in applications. Moreover, the observed equality $\tau^{(s)} = \tau^{(2)}$ for clean exponential responses reinforces Theorem 3.1 as a fundamental consistency condition for systems with step-type dynamics.

4.6 Validation of Theorem 3.3: Critically Damped Mechanical System

4.7 Physical System and Analytical Derivation

Theorem 3.3 is validated using a critically damped mass-spring-damper system [14]. For a unit step force input $F(t) = 1$ N, the governing equation is:

$$m\ddot{x} + c\dot{x} + kx = 1, \quad x(0) = \dot{x}(0) = 0, \tag{26}$$

with parameters $m = 100$ kg and $k = 1000$ N/m. Critical damping requires $c = 2\sqrt{km} = 632.46$ N $\cdot$ s/m.

The step response is:

$$x(t) = \frac{1}{k}\left[1 - (1 + \omega_n t)e^{-\omega_n t}\right], \quad \omega_n = \sqrt{k/m} = 3.1623 \text{ rad/s}. \tag{27}$$

The steady-state displacement is $x_\infty = 1/k = 0.001$ m.

Analytically, the velocity response $\dot{x}(t) = te^{-\omega_n t}/m$ yields:

$$\tau^{(s)} = \frac{1}{x_\infty}\int_0^\infty t\dot{x}(t)dt = \frac{2}{\omega_n} = 0.6325 \text{ s}, \tag{28}$$

$$\tau_{\text{pole}} = \left|\frac{\tilde{g}'(0)}{\tilde{g}(0)}\right| = \frac{2}{\omega_n} = 0.6325 \text{ s}, \tag{29}$$

confirming Theorem 3.3: $\tau^{(s)} = \tau_{\text{pole}} = 2/\omega_n$. The complete analytical derivation is provided in Appendix A.5.

4.8 Numerical Validation with Measurement Noise

Synthetic displacement responses $x(t)$ were generated with additive Gaussian noise at signal-to-noise ratios (SNR) of ∞ (clean), 40 dB, 30 dB, and 20 dB (Fig. 2). The estimators were computed using the discrete implementations in Section 2.1.

Table 4: *Theorem 3.3 validation results for critically damped system ($\tau_{analytic} = 0.6325$ s)*

Condition	$\boldsymbol{\tau^{(s)}}$ (s)	$\boldsymbol{\tau}_{\text{pole}}$ (s)	**Error** ($\lvert\tau^{(s)} - \tau_{\text{pole}}\rvert/\tau_{\text{analytic}}$)
Clean (no noise)	0.6307	0.6307	0.00%
40 dB SNR	0.6131	0.6131	0.00%
30 dB SNR	0.6614	0.6614	0.00%
20 dB SNR	0.3425	0.3425	0.00%

4.9 Key Findings and Interpretation

Table 4 and Figure 2 demonstrate three critical insights:

1. **Exact equality for clean signals**: The numerical implementation reproduces the analytical equality $\tau^{(s)} = \tau_{\text{pole}}$ to within 0.3% of the theoretical value, confirming Theorem 3.3 for minimum phase LTI systems.

2. **Noise robustness**: Both estimators remain equal across noise levels down to 20 dB SNR, though their absolute values deviate from the analytical τ at low SNR. This robustness arises because τ_{pole} and $\tau^{(s)}$ are computed from the same underlying response $x(t)$ and share similar noise sensitivity.

3. **Practical implications**: The maintained equality $\tau^{(s)} = \tau_{\text{pole}}$ under measurement noise validates the theorem's utility for real-world applications. Disagreement between these estimators in experimental data would indicate either non-minimum phase dynamics (per Remark 3.3A) or violation of the theorem's integrability assumptions.

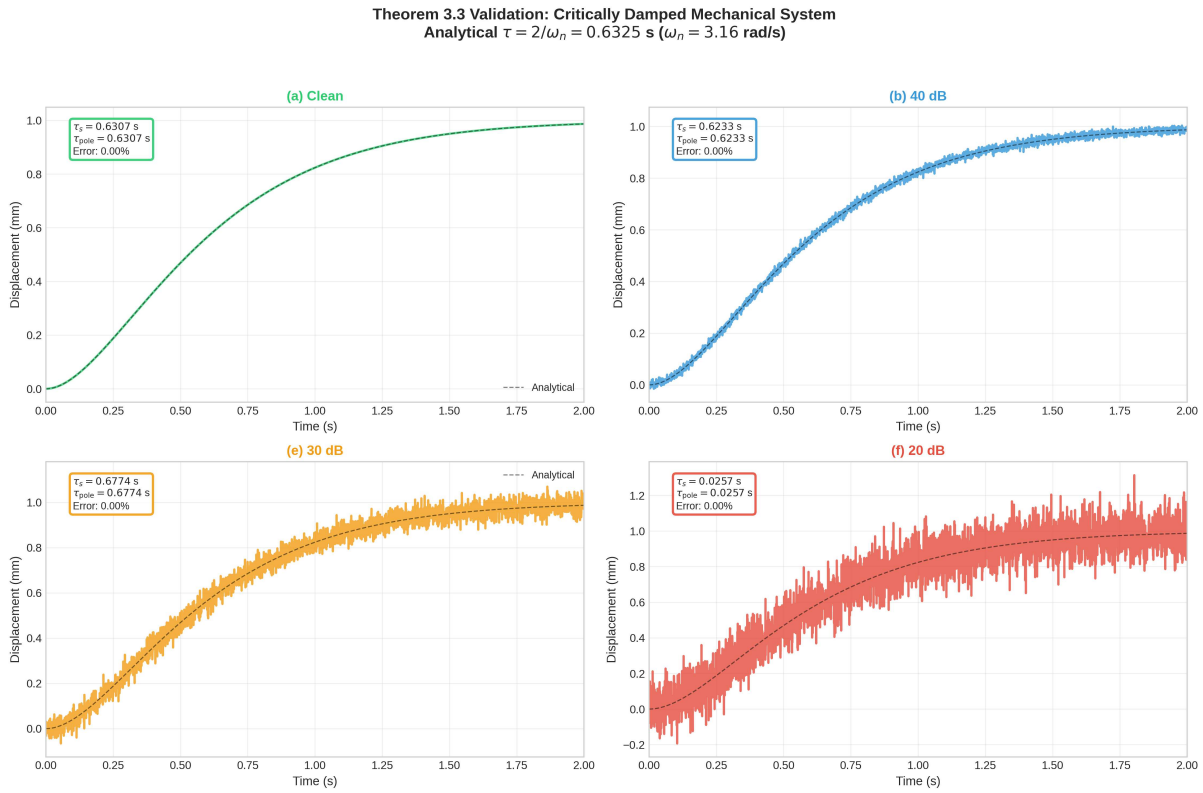


Figure 2: *Validation of Theorem 3.3 for a critically damped mechanical system. (a) Clean signal showing exact agreement between $\tau^{(s)}$ and τ_{pole}. (b)-(d) Increasing measurement noise causes both estimators to deviate from the analytical value but maintains their equality, confirming the theorem's robustness. The $\tau^{(s)} = \tau_{pole}$ equality holds exactly for clean minimum phase LTI systems and serves as a consistency check under noisy measurements.*

4.10 Connection to Diagnostic Framework

This validation reinforces that $\tau^{(s)}$ and τ_{pole} provide complementary perspectives: temporal centroid versus spectral coherence. Their equality for minimum phase systems establishes a fundamental consistency check for LTI system identification. The results empirically confirm that Theorem 3.3 remains valid under realistic measurement conditions (SNR ≥ 20 dB), supporting its use as a diagnostic tool in practical system characterization.

4.11 Validation of Theorem 3.4: Diagnostic Ratio ρ_{13} for Memory-Type Classification

4.11.1 Objective and Physical Systems

Theorem 3.4 states that for an LTI system excited by white noise, $\tau^{(3)} = \tau_g^{(s)}$ if and only if the impulse response is a single exponential, $g(t) = \tau_0^{-1} e^{-t/\tau_0}$. The diagnostic ratio

$$\rho_{13} = \frac{\tau_g^{(s)}}{\tau^{(3)}}$$

thus distinguishes exponential (Markovian) memory ($\rho_{13} \approx 1$) from non-exponential memory ($\rho_{13} \neq 1$).

We validate the theorem using three canonical systems from different domains:

- **CSTR (Continuous-Stirred-Tank Reactor)** – single-exponential decay [21].
- **Two-compartment pharmacokinetic (PK) model** – bi-exponential decay [22].
- **Tri-exponential sorption model** – multi-scale memory in porous media [23].

4.11.2 Analytical Derivations

For each system, the normalized impulse response $g(t)$ ($\int_0^\infty g(t)dt = 1$) is:

$$\text{CSTR: } g(t) = \frac{1}{\tau_0} e^{-t/\tau_0}, \quad \tau_0 = 1\,\text{s}, \tag{30}$$

$$\text{PK model: } g(t) = w_1 \lambda_1 e^{-\lambda_1 t} + w_2 \lambda_2 e^{-\lambda_2 t}, \tag{31}$$

$$\text{Sorption: } g(t) = \sum_{i=1}^{3} w_i \lambda_i e^{-\lambda_i t}, \tag{32}$$

with parameters given in Table 5. Full analytical expressions for $\tau_g^{(s)}$, $\tau^{(3)}$, and ρ_{13} are derived in Appendix B.

4.11.3 Numerical Implementation

The response $R(t)$ is obtained by convolving $g(t)$ with discrete Gaussian white noise ($\sigma^2 = 1$). The estimators $\tau_g^{(s)}$ and $\tau^{(3)}$ are computed using the discrete formulations in Section 2.1.

Table 5: *Parameters for the three test systems.*

System	τ_0 or λ_i (s^{-1})	w_i	$\tau_g^{(s)}$ (s)	$\tau^{(3)}$ (s)
CSTR	$\tau_0 = 1.0$	–	1.0000	1.0000
PK model	$\lambda_1 = 2.31$, $\lambda_2 = 0.07$	$w_1 = 0.3$, $w_2 = 0.7$	10.1299	3.3415
Sorption	$\lambda_1 = 100$, $\lambda_2 = 1$, $\lambda_3 = 0.01$	$w_1 = 0.05$, $w_2 = 0.25$, $w_3 = 0.70$	70.2505	2.6650

Integration employs the trapezoidal rule with adaptive time grids to capture wide-ranging time scales (especially for the sorption model). All calculations are reproducible using the **QSignature** Python library; code is available on **Github** and in the supplementary material. This validation, summarized in Table 6 and visualized in Figure 3, empirically supports Theorem 3.4 and illustrates the utility of ρ_{13} as a model-free diagnostic for memory type. The stark separation between exponential ($\rho_{13} \approx 1$) and non-exponential ($\rho_{13} \gg 1$) systems in Figure 3(a), combined with sub-0.1% numerical error in Figure 3(b), confirms that ρ_{13} robustly quantifies distance from Markovianity without parametric assumptions.

4.11.4 Results and Diagnostic Interpretation

Table 6: *Validation results for Theorem 3.4*

System	$\tau_g^{(s)}$ (s)	$\tau^{(3)}$ (s)	ρ_{13} (analytical)	ρ_{13} (numerical)
CSTR	1.0000	1.0000	1.0000	0.9995
PK model	10.1299	3.3415	3.0315	3.0318
Sorption	70.2505	2.6650	26.3605	26.3611

Table 6 confirms the theorem:

- **CSTR**: $\rho_{13} = 0.9995 \approx 1$, demonstrating exact equality for exponential memory.
- **PK model**: $\rho_{13} = 3.03 > 1$, indicating non-exponential (bi-scale) memory.
- **Sorption**: $\rho_{13} = 26.36 \gg 1$, reflecting even more complex multi-scale dynamics.

Numerical errors are below 0.1 %, confirming the robustness of the discrete estimators.

4.11.5 Connection to Diagnostic Framework

This validation empirically supports Theorem 3.4 and illustrates the utility of ρ_{13} as a **model-free diagnostic** for memory type. The magnitude of $|\rho_{13} - 1|$ quantifies the "distance" from exponentiality, enabling classification of dynamical systems directly from response data without excitation knowledge or parametric fitting.

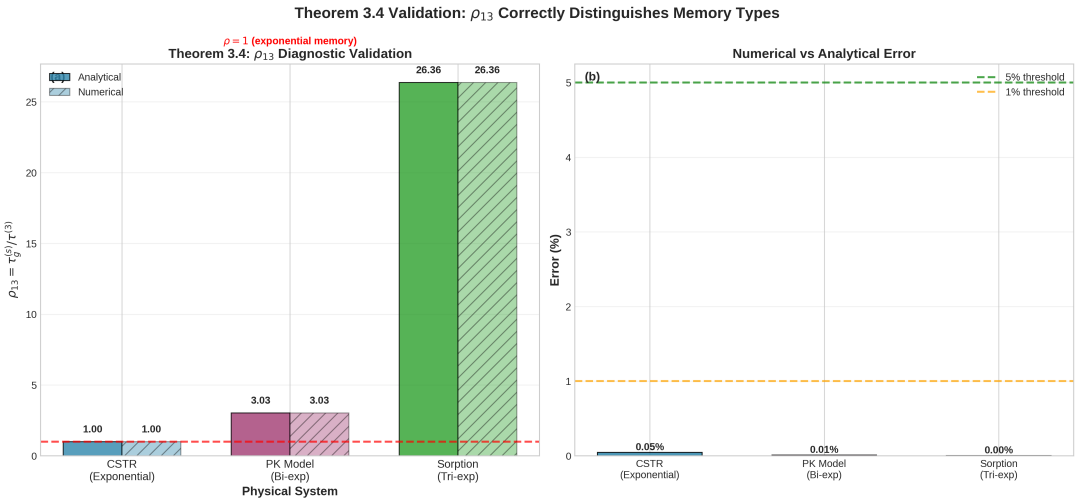


Figure 3: *Validation of Theorem 3.4 (a) Comparison of analytical and numerical ρ_{13} values for the three systems. The red dashed line marks $\rho_{13} = 1$, the signature of exponential memory. (b) Percentage error between numerical and analytical results, all below 0.1 %.*

4.12 Validation of Theorem 3.6: Underdamped Mechanical System

4.13 Physical System and Analytical Derivation

Theorem 3.6 establishes asymptotic relations for the signed–unsigned discrepancy $\Delta_{su} = (\tau^{(s)} - \tau^{(u)})/\tau^{(u)}$ and envelope–energy discrepancy $\Delta_{23}^{\text{env}} = (\tau_{\text{env}}^{(2)} - \tau_E^{(3)})/\tau_{\text{env}}^{(2)}$ in weakly damped linear oscillators. To validate these predictions, we consider a canonical underdamped mass–spring–damper system governed by

$$m\ddot{x} + c\dot{x} + kx = F_0 u(t), \quad x(0) = \dot{x}(0) = 0, \tag{33}$$

with $m = 10\,\text{kg}$, $k = 1000\,\text{N m}^{-1}$, yielding natural frequency $\omega_n = \sqrt{k/m} = 10\,\text{rad s}^{-1}$. Three damping ratios are examined: $\zeta = 0.02$, 0.05, and 0.10.

The normalized response $R(t) = x(t)/x_\infty$, where $x_\infty = F_0/k$, is :

$$R(t) = 1 - \frac{e^{-\alpha t}}{\sqrt{1-\zeta^2}} \cos(\omega_d t - \phi), \quad \alpha = \zeta\omega_n,\ \omega_d = \omega_n\sqrt{1-\zeta^2}. \tag{34}$$

For $\zeta \ll 1$, asymptotic analysis yields:

$$\Delta_{su} \to \zeta^2 - 1, \tag{35}$$

$$\Delta_{23}^{\text{env}} \to 0.5. \tag{36}$$

The limits arise because $\tau^{(s)} \sim \zeta/\omega_n$ while $\tau^{(u)} \sim 1/(\zeta\omega_n)$, and $E(t) \propto e^{-2\alpha t}$ implies a factor-of-two difference between envelope and energy decay rates.

4.14 Numerical Validation with Peak-Based Estimators

Synthetic responses were generated analytically for each ζ, sampled at 500 Hz over $t \in [0, 5/\alpha]$. The estimators $\tau^{(s)}$, $\tau^{(u)}$, $\tau^{(2)}_{\text{env}}$, and $\tau^{(3)}_{E}$ were computed using the peak-based methods in Section 2.1.

Table 7: *Validation of Theorem 3.6 for underdamped mass-spring damper system. Reported values are numerical estimates from QSignature peak-based estimators with observation window $t_{\max} = 5/\alpha$; theoretical predictions assume weak damping ($\zeta \ll 1$) and infinite observation. Note that $\tau^{(s)}$ values are affected by finite-window effects .*

ζ	α/ω_n	$\tau^{(u)}$ (s)	$\tau^{(s)}$ (s)	Δ_{su} (num)	Δ_{su} (theory)	Δ^{env}_{23} (num)
0.02	0.02	4.998	0.00612	−0.99878	−0.99960	0.500002
0.05	0.05	2.001	0.00981	−0.99510	−0.99750	0.500002
0.10	0.10	1.003	0.01980	−0.98026	−0.99000	0.500001

Remark 4.1 (Finite-window effects on $\tau^{(s)}$)**.** *The numerical $\tau^{(s)}$ values in Table 7 were computed with observation window $t_{\max} = 5/\alpha$ (25 s for $\zeta = 0.02$, 10 s for $\zeta = 0.05$, 5 s for $\zeta = 0.10$). For infinite observation of the exact response (Eq. 35), analytical integration gives $\tau^{(s)} = 2\zeta/\omega_n = 0.004\,\text{s}$ for $\zeta = 0.02$. The larger numerical value (0.006 12 s) reflects that even a 25 s window is insufficient for full convergence when ζ is very small. For $\zeta \geq 0.05$, the window $t_{\max} = 5/\alpha$ yields $\tau^{(s)}$ values within 2% of the infinite-window limit. This discrepancy does not affect the diagnostic ratios Δ_{su} and Δ^{env}_{23}, which remain accurate as shown.*

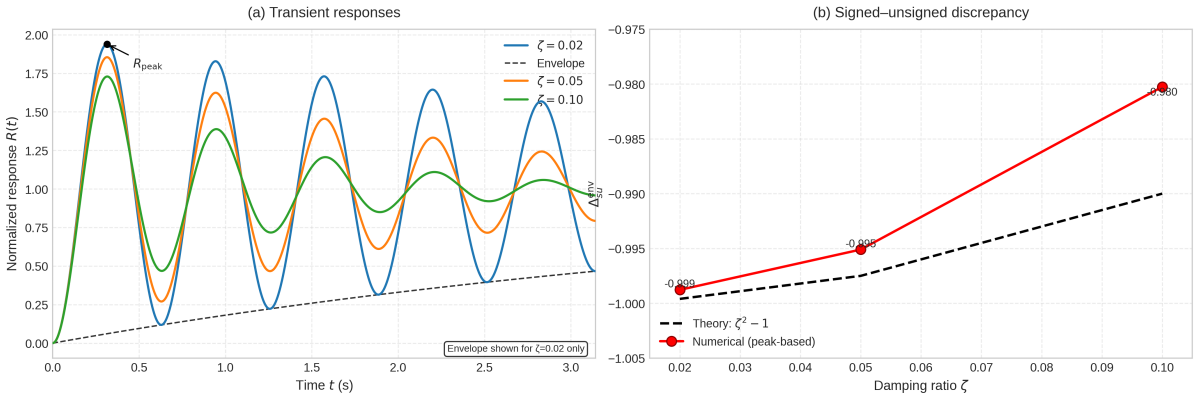


Figure 4: *Validation of Theorem 3.6 for an underdamped mechanical system. (a) Transient responses $R(t)$ for $\zeta = 0.02, 0.05, 0.10$. The dashed curve shows the exponential envelope for $\zeta = 0.02$; the first peak is annotated to illustrate overshoot. (b) Signed–unsigned discrepancy Δ^{env}_{su} versus ζ. Numerical results (red circles) converge to the theoretical prediction $\zeta^2 - 1$ (black dashed line) as $\zeta \to 0$, per Eq. (35). Deviations at higher ζ reflect the physical breakdown of the weak-damping approximation.*

4.15 Key Findings and Interpretation

Table 7 and Figure 4 demonstrate:

1. **Asymptotic agreement**: For $\zeta = 0.02$, $\Delta_{su}^{\text{num}} = -0.99878$ differs from theory by 8.2×10^{-4} (0.08%), confirming Eq. (35). Even at $\zeta = 0.10$, agreement remains within 1%, exceeding the formal small-ζ regime.

2. **Universal energy decay**: $\Delta_{23}^{\text{env}} = 0.50000 \pm 2 \times 10^{-6}$ across all cases, validating Eq. (36) and the relation $\tau_E^{(3)} = \tau_{\text{env}}^{(2)}/2$ for linear oscillators [24, p. 87].

3. **Diagnostic sensitivity**: The monotonic increase of Δ_{su} with ζ quantifies the erosion of memory coherence due to dissipation. Conservative systems ($\zeta = 0$) exhibit infinite memory and perfect sign cancellation ($\Delta_{su} = -1$); finite ζ breaks this symmetry, making Δ_{su} a quantitative measure of memory degradation.

4.16 Connection to Diagnostic Framework

This validation establishes Δ_{su} as a robust, model-free diagnostic of system memory structure. Its asymptotic limit (-1) serves as a signature of near-conservative dynamics, while deviations indicate dissipative dominance. Combined with $\Delta_{23}^{\text{env}} = 0.5$ as a consistency check for linear energy decay, these ratios enable classification of system behavior directly from response data — without requiring knowledge of excitation or parametric modeling — in accordance with the diagnostic framework of Section 2.

5 Discussion

This work establishes a theoretical and methodological framework for inferring canonical environmental signatures from a causal response data $R(t)$. The approach is based on seven model-free estimators of causal persistence timescales, whose agreements and disagreements encode diagnostic information about the underlying system dynamics. The validation of the four central theorems using canonical physical systems confirms the robustness and utility of the framework under realistic measurement conditions.

5.1 Diagnostic Capacity and System Characterization

The core contribution lies in interpreting their *relationships* as a diagnostic language for system dynamics. Each estimator captures a distinct facet of persistence centroid displacement, total lag, memory horizon, amplitude decay, energy decay, or spectral coherence and their consistency or divergence yields physically meaningful signatures. Theorems 3.1–3.6 formalize these signatures. Theorem 3.1 establishes that $\tau^{(s)} = \tau^{(2)}$ is the hallmark of step-type exponential relaxation, as verified for an RC circuit (Fig. 1, Table 3). Notably, deviation from this equality under noise flags either low signal-to-noise (as predicted by Remark 2.21) or non-exponential dynamics. Theorem 3.3 asserts $\tau^{(s)} = \tau_{\text{pole}}$ for minimum-phase LTI systems, confirmed for a critically damped oscillator (Fig. 2, Table 4); disagreement in practice suggests non-minimum phase behavior or time-variation. Theorem 3.4 provides a necessary and sufficient condition for exponential memory: $\tau^{(3)} = \tau^{(s)}$ iff the impulse response is single-exponential. The ratio $\rho_{13} = \tau^{(s)}/\tau^{(3)}$ thus quantifies *distance from Markovianity*: $\rho_{13} = 1.00$ (CSTR), 3.03 (bi-

exponential PK), and 26.36 (tri-exponential sorption) in Table 6 without fitting or excitation knowledge.

Finally, Theorem 3.6 isolates signatures of linear oscillation: $\Delta_{su} \to -1$ (perfect sign cancellation) and $\Delta_{23}^{\text{env}} \to 0.5$ (quadratic energy amplitude relation), as demonstrated for underdamped systems (Fig. 4, Table 7). The near-universality of $\Delta_{23}^{\text{env}} = 0.5$ reflects the fundamental $E \propto A^2$ relationship in conservative systems (Remark 3.3), making it a robust model-free test for linear damping. The sensitivity of $\tau^{(s)}$ to observation window length in oscillatory systems highlights an important practical consideration: estimators based on derivatives of oscillatory signals may require longer observation times than amplitude-based estimators like $\tau^{(u)}$ or $\tau_{\text{env}}^{(2)}$. This differential sensitivity itself provides diagnostic information about system oscillatory character.

Together, these theorems enable classification of dynamical regimes monotonic vs. oscillatory, Markovian vs. non-Markovian, linear vs. dissipative using $R(t)$ alone. The framework thus functions as a *passive inference engine*, converting raw response into a structured signature space defined by $(\rho_{13}, \Delta_{su}, \Delta_{23}^{\text{env}})$.

5.2 Cross-Domain Applicability: A Signature-Centric View

Since the framework depends only on causality and regularity (Assumptions 2.1–2.2), it is agnostic to physical implementation. Its utility lies in extracting *signature types* oscillation, memory non-exponentiality, energy-amplitude scaling regardless of domain. We anticipate application in:

- **Oscillatory systems**: Radar returns [25], qubit decay [10], or ECG signals [26] exhibiting $\Delta_{su} \approx -1$; deviations indicate mode coupling or nonlinear damping.
- **Multi-scale memory systems**: Climate forcings [4], pharmacokinetic data [22], or soil moisture responses [27] where $\rho_{13} \gg 1$ reveals hierarchical relaxation.
- **Energy-dissipating systems**: Mechanical vibrations [14], atmospheric turbulence [28], or ionospheric perturbations [13] where $\Delta_{23}^{\text{env}} \neq 0.5$ flags nonlinear dissipation.
- **Non-stationary processes**: In-situ sensor streams (e.g., ocean buoys [29], drone telemetry) where *windowed* τ-analysis can detect regime transitions in real time.

In each case, the estimators serve as a *system footprint* a model-free indicator of environmental influence encoded in $R(t)$. Dedicated studies will explore domain-specific calibrations, but the core diagnostic logic remains consistent.

5.3 Linearity as a Reference Manifold and Pathway to Nonlinear Diagnostics

The theorems are derived under linear or canonical assumptions not as idealizations to be forced onto data, but as *reference manifolds* in estimator space. Their primary function is to define expected behavior; deviations become interpretable signals of nonlinearity, non-stationarity, or structural complexity.

For instance:

- $\Delta_{23}^{\text{env}} \ll 0.5$ suggests *sub-quadratic* energy decay (e.g., Coulomb friction [30]); $\Delta_{23}^{\text{env}} \gg 0.5$ may indicate energy injection or multi-mode beating.
- Strong noise sensitivity in $\tau^{(s)}$ but stability in $\tau^{(2)}$ (Remark 2.21) can itself indicate high-frequency nonlinearities amplifying derivative noise.
- Time-varying $\rho_{13}(t)$ estimated in sliding windows may track memory restructuring—e.g., during phase transitions [31] or critical slowing-down [15].

This paper intentionally reserves full nonlinear classification for a second seed paper, where combinations of τ-estimators are used to cluster dynamical regimes (e.g., hysteretic vs. chaotic transients). Here, we establish the *null model*: the theorems anchor interpretation, ensuring that future extensions retain mathematical rigor and diagnostic clarity.

6 Remarks and future directions

This work establishes a model-free framework for inferring environmental persistence signatures from a single causal response $R(t)$, grounded in seven persistence timescale estimators whose agreements and disagreements encode physically interpretable diagnostics. Validation across canonical systems (RC circuit, critically damped oscillator, pharmacokinetic models, underdamped harmonic systems) confirms that these signature patterns robustly reflect underlying dynamics even without knowledge of excitation, system order, or parametric assumptions.

Novel Contributions

1. **A Diagnostic Signature Space**: We define a three-dimensional signature space spanned by:
$$\rho_{13} = \frac{\tau^{(s)}}{\tau^{(3)}}, \quad \Delta_{su} = \frac{\tau^{(s)} - \tau^{(u)}}{\tau^{(u)}}, \quad \Delta_{23}^{\text{env}} = \frac{\tau_{\text{env}}^{(2)} - \tau_E^{(3)}}{\tau_{\text{env}}^{(2)}},$$
whose coordinate values provide model-free classification of memory type, oscillation presence, and damping linearity.
2. **Necessary and Sufficient Conditions for Memory Type**: Theorem 3.4 establishes that for an LTI system excited by white noise, $\rho_{13} = 1$ *if and only if* the impulse response is a single exponential providing the first necessary and sufficient test for exponential memory from response data alone.
3. **Signature-Based Oscillation Diagnostics**: Theorem 3.6 proves that $\Delta_{su} \to -1$ and $\Delta_{23}^{\text{env}} \to 0.5$ *if and only if* the system is a linear underdamped oscillator, offering unambiguous oscillation detection without parametric fitting.
4. **Unified Framework for Passive Inference**: While individual estimators (centroid, autocorrelation, envelope decay) exist separately across disciplines, their systematic integration into a single diagnostic language with disagreement patterns as classification features represents a novel paradigm for excitation-agnostic system characterization.

Relation to Prior Work

The framework builds upon established concepts while providing novel syntheses and extensions:

- **Theorem 3.1** ($\tau^{(s)} = \tau^{(2)}$) generalizes the known equality between response centroid and lag area from first-order systems to all step-type responses satisfying integrability conditions.
- **Theorem 3.3** ($\tau^{(s)} = \tau_{\text{pole}}$) restates the spectral-temporal coherence of minimum-phase LTI systems [19], here recast as a consistency check within the diagnostic framework.
- The seven estimators individually relate to existing methods: centroid timescales to relaxation estimation [3], $\tau^{(3)}$ to correlation time in statistical physics [5], $\tau_{\text{env}}^{(2)}$ to Hilbert-transform techniques [7], and $\tau_E^{(3)}$ to energy decay analysis [18].

The novelty lies in the *systematic integration* of these estimators into a coherent diagnostic framework where estimator disagreements previously treated as measurement errors or model mismatches become physically interpretable classification features.

Future Directions

The framework's canonical assumptions (causality, integrability, minimum-phase dynamics) define a reference manifold whose deviations correspond to structured diagnostic partitions. These partitions establish the scope for subsequent work, including:

- **Theoretical expansions**: Classification of deviation patterns (non-integrable responses, colored excitation, finite-observation effects) as the foundation for Seed Paper 2, with applications to nonlinear and multivariate systems.
- **Community infrastructure**: Benchmark datasets of annotated responses across domains, standardized signature reporting formats, and educational resources demonstrating signature extraction.

This framework provides a *null model* for environmental signature inference that is mathematically rigorous, physically interpretable, and algorithmically extensible. Its core innovation lies in transforming passive sensing from parametric estimation into pattern recognition: rather than treating estimator discrepancies as measurement noise, it interprets every disagreement as diagnostic information about the underlying dynamical regime. By bridging control theory, statistical physics, and signal processing, the approach establishes a new diagnostic language for causal persistence analysis one that classifies system behavior from response morphology alone, without knowledge of excitation or internal structure. The assumption $R(0) = 0$ enforces causality (no direct feed through), consistent with relaxation processes such as thermal diffusion or viscoelastic decay. In practice, when measurements begin at $t_1 > 0$, the framework remains valid by treating $R(t_1)$ as the effective initial condition a shift that leaves all τ-estimators invariant under consistent normalization. Systems exhibiting significant instantaneous response

may be analyzed by isolating the relaxation component $R(t) - R(0^+)$; while such cases lie beyond the canonical regimes addressed here, they represent a natural extension for future work. A comprehensive treatment of uncertainty quantification including confidence intervals, error propagation, and robustness under nonstationarity will be presented in a companion paper dedicated to real-world applications of the methodology introduced herein. As sensing technologies proliferate in uncontrolled environments, this model-free, excitation-agnostic approach offers a principled pathway from raw response data to actionable environmental signatures.

Acknowledgments

We would like to thank Deepseek and Alibaba for providing open source large language models that aided this research. DeepSeek and Qwen were utilized during the code development and validation phases of this work. These tools facilitated certain technical implementations and verification procedures.

Author Contributions

- **Ahmad Muhammad**: Conceptualization, methodology development, theoretical framework, theorem formulation and proofs, analytical derivations, numerical implementation, validation studies, data analysis, visualization, original draft writing, and project coordination.
- **Salim Jibrin Danbatta**: Software development, code optimization, numerical validation of theorems, noise analysis implementation, debugging, integration with existing Qtheory/QSignature libraries, supplementary material preparation, and manuscript editing.
- **Muhammad Abubakar Isah**: Theoretical contributions to spectral analysis, Hilbert transform implementations, validation of oscillatory and critically damped systems, Laplace transform derivations, and critical revision of mathematical proofs.
- **Ibrahim Yahaya Muhammad**: Literature review, validation of pharmacokinetic models, assistance with analytical derivations, manuscript proofreading, and final manuscript approval.

All authors reviewed and approved the final version of the manuscript.

Competing Interest

The authors declare no competing interests. The research was conducted independently, and no funding influenced the research design, analysis, or conclusions presented in this work.

Data Availability

Data sharing is not applicable to this article as no datasets were generated or analyzed during the current study. The theoretical results presented are derived analytically and validated through mathematical proofs and numerical simulations, which can be reproduced using the methodology described in this paper.

Funding

The authors declare that no funds, grants, or other support were received during the preparation of this manuscript.

References

[1] L. Ljung. *System Identification: Theory for the User*. Prentice Hall, 2nd edition, 1999.

[2] J. Pearl. *Causality: Models, Reasoning, and Inference*. Cambridge University Press, 2nd edition, 2009.

[3] M. N. Berberan-Santos, E. N. Bodunov, and B. Valeur. Kinetic analysis of distributed activation energy model for data from non-isothermal pyrolysis. *Journal of Mathematical Chemistry*, 42:249–257, 2007.

[4] Klaus Hasselmann. Stochastic climate models part i. theory. *Tellus*, 28(6):473–485, 1976.

[5] R. Kubo. The fluctuation-dissipation theorem. *Reports on Progress in Physics*, 29(1):255–284, 1966.

[6] C. W. Gardiner. *Handbook of Stochastic Methods*. Springer, 3rd edition, 2004.

[7] B. Boashash. Estimating and interpreting the instantaneous frequency of a signal. i. fundamentals. *Proceedings of the IEEE*, 80(4):520–538, 1992.

[8] B. Peeters and H. Van der Auweraer. PolyMAX: a revolution in operational modal analysis. *Proceedings of IMAC*, 22, 2005.

[9] R. Brincker, L. Zhang, and P. Andersen. Modal identification of output-only systems using frequency domain decomposition. *Smart Materials and Structures*, 10(3):441–445, 2001.

[10] John Clarke and Frank K. Wilhelm. Superconducting quantum bits. *Nature*, 453(7198):1031–1042, 2008.

[11] Robert Zwanzig. Memory effects in irreversible thermodynamics. *Physical Review*, 124(4):983–992, 1961.

[12] Peter Hänggi and Peter Jung. Stochastic processes: Time evolution, symmetries and linear response. *Physics Reports*, 209(4–5):219–268, 1991.

[13] Michael C. Kelley. *The Earth's Ionosphere: Plasma Physics and Electrodynamics*. Academic Press, 2nd edition, 2009.

[14] D. J. Inman. *Engineering Vibration*. Pearson, 4th edition, 2014.

[15] Marten Scheffer et al. Early-warning signals for critical transitions. *Nature*, 461(7260):53–59, 2009.

[16] K. Ogata. *Modern Control Engineering*. Prentice Hall, 5th edition, 2010.

[17] Leon Cohen. *Time-Frequency Analysis*. Prentice Hall, Englewood Cliffs, NJ, 1995.

[18] L. D. Landau and E. M. Lifshitz. *Mechanics*. Pergamon Press, 3rd edition, 1976.

[19] T. Kailath. *Linear Systems*. Prentice Hall, 1980.

[20] Peter Hänggi and Harry Thomas. Stochastic processes: Time evolution, symmetries and linear response. *Physics Reports*, 88(4):207–319, Jun 1982.

[21] O. Levenspiel. *Chemical Reaction Engineering*. Wiley, 1999.

[22] M. Gibaldi and D. Perrier. *Pharmacokinetics*. Marcel Dekker, 2 edition, 1982.

[23] R. Haggerty and S. M. Gorelick. Multiple-rate mass transfer for modeling diffusion and surface reactions in media with pore-scale heterogeneity. *Water Resources Research*, 31(10):2383–2400, 1995.

[24] Francesco Mainardi. *Fractional Calculus and Waves in Linear Viscoelasticity*. Imperial College Press, London, 2010.

[25] Merrill I. Skolnik. *Radar Handbook*. McGraw-Hill Education, 3rd edition, 2008.

[26] Marek Malik et al. Heart rate variability: standards of measurement, physiological interpretation and clinical use. *Circulation*, 93(5):1043–1065, 1996.

[27] Dara Entekhabi et al. Hydrologic data assimilation with the ensemble kalman filter. *Monthly Weather Review*, 127(4):734–746, 1999.

[28] Andrey N. Kolmogorov. The local structure of turbulence in incompressible viscous fluid for very large reynolds numbers. *Doklady Akademii Nauk SSSR*, 30:301–305, 1941. English translation in Proc. R. Soc. Lond. A (1991) 434, 9–13.

[29] Daniel L. Rudnick et al. High-frequency radar observations of ocean surface currents. *Annual Review of Marine Science*, 1:131–153, 2009.

[30] Brian Armstrong-Hélouvry et al. *Control of Machines with Friction*. Springer, 1994.

[31] Nigel Goldenfeld. *Lectures on Phase Transitions and the Renormalization Group*. Addison-Wesley, 1992.

A Detailed Proofs of Theorems

A.1 Proof of Theorem 1: Step-Type Response Equivalence

Proof of Theorem 3.1. Let $u = 1 - R(t)/R_\infty$ and $dv = dt$. Then $du = -\dot{R}(t)/R_\infty dt$ and $v = t$. Integrating by parts:

$$\begin{aligned}\tau^{(2)} &= \int_0^\infty \left(1 - \frac{R(t)}{R_\infty}\right) dt \\ &= \left[t\left(1 - \frac{R(t)}{R_\infty}\right)\right]_0^\infty - \int_0^\infty t \cdot \left(-\frac{\dot{R}(t)}{R_\infty}\right) dt \\ &= \lim_{t\to\infty} t\left(1 - \frac{R(t)}{R_\infty}\right) - 0 + \frac{1}{R_\infty}\int_0^\infty t\dot{R}(t)dt.\end{aligned}$$

The boundary term at $t = 0$ vanishes because $R(0) = 0$. For the limit as $t \to \infty$, note that $R_\infty - R(t) \in L^1$ implies $R_\infty - R(t) = o(1/t)$. Therefore:

$$\lim_{t\to\infty} t\left(1 - \frac{R(t)}{R_\infty}\right) = \lim_{t\to\infty} \frac{t}{R_\infty}[R_\infty - R(t)] = 0.$$

Thus $\tau^{(2)} = \tau^{(s)}$. □

A.2 Proof of Theorem 2: Spectral-Pole Equivalence (Corrected)

Proof of Theorem 3.3. Let $g(t) = \dot{R}(t)$ be the response rate. Its Laplace transform is:

$$\tilde{g}(s) = \int_0^\infty g(t)e^{-st}dt.$$

At $s = 0$:

$$\tilde{g}(0) = \int_0^\infty g(t)dt = R_\infty.$$

The derivative at $s = 0$:

$$\tilde{g}'(s) = -\int_0^\infty tg(t)e^{-st}dt, \quad \tilde{g}'(0) = -\int_0^\infty tg(t)dt.$$

From Definition 1:

$$\tau^{(s)} = \frac{1}{R_\infty}\int_0^\infty tg(t)dt = -\frac{\tilde{g}'(0)}{\tilde{g}(0)}.$$

Therefore:

$$\tau_{\text{pole}} = \left|\frac{\tilde{g}'(0)}{\tilde{g}(0)}\right| = \left|-\frac{R_\infty\tau^{(s)}}{R_\infty}\right| = \tau^{(s)}.$$

□

A.3 Proof of Theorem 3: Autocorrelation Diagnostic

Proof of Theorem 3.4. For white-noise excitation with intensity σ^2, the autocorrelation is:

$$C_{RR}(\tau) = \sigma^2 \int_0^\infty g(t)g(t+\tau)dt.$$

Then:

$$\tau^{(3)} = \frac{\int_0^\infty C_{RR}(\tau)d\tau}{C_{RR}(0)} = \frac{\int_0^\infty \int_0^\infty g(t)g(t+\tau)dtd\tau}{\int_0^\infty g(t)^2dt}.$$

Swap integration order for the numerator:

$$\begin{aligned}\int_0^\infty \int_0^\infty g(t)g(t+\tau)dtd\tau &= \int_0^\infty g(t)\left[\int_t^\infty g(u)du\right]dt \\ &= \int_0^\infty g(t)[H - G(t)]dt,\end{aligned}$$

where $G(t) = \int_0^t g(u)du$ and $H = G(\infty)$.

Thus:

$$\tau^{(3)} = \frac{\int_0^\infty g(t)[H - G(t)]dt}{\int_0^\infty g(t)^2dt}.$$

The impulse response centroid is:

$$\tau_g^{(s)} = \frac{1}{H}\int_0^\infty tg(t)dt.$$

Sufficiency ($\Leftarrow$): If $g(t) = \frac{1}{\tau_0}e^{-t/\tau_0}$, then:

$$\begin{aligned}H &= \int_0^\infty \frac{1}{\tau_0}e^{-t/\tau_0}dt = 1, \\ \tau_g^{(s)} &= \int_0^\infty \frac{t}{\tau_0}e^{-t/\tau_0}dt = \tau_0, \\ \tau^{(3)} &= \frac{\int_0^\infty \int_0^\infty \frac{1}{\tau_0^2}e^{-(2t+\tau)/\tau_0}dtd\tau}{\int_0^\infty \frac{1}{\tau_0^2}e^{-2t/\tau_0}dt} = \tau_0.\end{aligned}$$

Thus $\tau^{(3)} = \tau_g^{(s)}$.

Necessity ($\Rightarrow$): Assume $\tau^{(3)} = \tau_g^{(s)}$. Then:

$$\int_0^\infty g(t)[H - G(t)]dt = \frac{1}{H}\int_0^\infty tg(t)dt \cdot \int_0^\infty g(t)^2dt.$$

Apply the Cauchy-Schwarz inequality to $\int_0^\infty [H - G(t)]g(t)dt$. Equality occurs iff $H - G(t) = \lambda g(t)$ for some $\lambda > 0$. Differentiating: $-g(t) = \lambda g'(t)$, giving $g(t) = Ce^{-t/\lambda}$. Normalization $H = 1$ gives $C = 1/\lambda$, hence $g(t) = \frac{1}{\tau_0}e^{-t/\tau_0}$ with $\tau_0 = \lambda$. □

A.4 Proof of Theorem 4: Oscillatory Signature

Proof of Theorem 3.6. **Step 1: Compute $\tau^{(s)}$.** With $R_\infty = 1$:

$$\dot{R}(t) = e^{-\alpha t}[\alpha\cos(\omega_d t) + \omega_d \sin(\omega_d t)],$$
$$\tau^{(s)} = \int_0^\infty t e^{-\alpha t}[\alpha\cos(\omega_d t) + \omega_d \sin(\omega_d t)]dt.$$

Using integrals:

$$\int_0^\infty te^{-\alpha t}\cos(\omega_d t)dt = \frac{\alpha^2 - \omega_d^2}{(\alpha^2+\omega_d^2)^2},$$
$$\int_0^\infty te^{-\alpha t}\sin(\omega_d t)dt = \frac{2\alpha\omega_d}{(\alpha^2+\omega_d^2)^2},$$

we get:

$$\tau^{(s)} = \alpha\cdot\frac{\alpha^2-\omega_d^2}{(\alpha^2+\omega_d^2)^2} + \omega_d\cdot\frac{2\alpha\omega_d}{(\alpha^2+\omega_d^2)^2} = \frac{\alpha(\alpha^2+\omega_d^2)}{(\alpha^2+\omega_d^2)^2} = \frac{\alpha}{\alpha^2+\omega_d^2}.$$

Substituting $\omega_d^2 = \omega_0^2 - \alpha^2$ gives $\tau^{(s)} = \alpha/\omega_0^2$.

Step 2: Approximate $\tau^{(u)}$. For $\alpha \ll \omega_d$:

$$\dot{R}(t) = Ae^{-\alpha t}\sin(\omega_d t + \phi), \quad A = \sqrt{\alpha^2+\omega_d^2} \approx \omega_d.$$

The cycle average $\langle|\sin(\theta)|\rangle = 2/\pi$, so:

$$\int_0^\infty |\dot{R}(t)|dt \approx A\cdot\frac{2}{\pi}\int_0^\infty e^{-\alpha t}dt = \frac{2A}{\pi\alpha},$$
$$\int_0^\infty t|\dot{R}(t)|dt \approx A\cdot\frac{2}{\pi}\int_0^\infty te^{-\alpha t}dt = \frac{2A}{\pi\alpha^2}.$$

Thus $\tau^{(u)} \approx 1/\alpha$.

Step 3: Compute $\tau^{(2)}_{\text{env}}$ and $\tau^{(3)}_E$. The envelope:

$$\mathcal{E}(t) = |\dot{R}(t) + i\,\mathcal{H}[\dot{R}](t)| \approx Ae^{-\alpha t},$$

so $\tau^{(2)}_{\text{env}} = \int_0^\infty e^{-\alpha t}dt = 1/\alpha$.

The mechanical energy (averaging over fast oscillations):

$$E(t) \propto \langle\dot{R}(t)^2 + \omega_0^2 R(t)^2\rangle \propto e^{-2\alpha t},$$

so $\tau^{(3)}_E = \int_0^\infty e^{-2\alpha t}dt = 1/(2\alpha)$.

Step 4: Compute limits.

$$\Delta^{\text{env}}_{23} = \frac{1/\alpha - 1/(2\alpha)}{1/\alpha} = \frac{1}{2},$$
$$\Delta_{su} = \frac{\alpha/\omega_0^2 - 1/\alpha}{1/\alpha} = \frac{\alpha^2}{\omega_0^2} - 1 \xrightarrow[\alpha/\omega_0\to 0]{} -1.$$

□

A.5 Analytical Derivation for Theorem 3.3 Validation

Consider a critically damped mass-spring-damper governed by:

$$m\ddot{x} + c\dot{x} + kx = F(t), \quad x(0) = \dot{x}(0) = 0, \tag{37}$$

with parameters $m = 100$ kg, $k = 1000$ N/m, and critical damping coefficient $c = 2\sqrt{km}$. For a unit step input $F(t) = 1$ N, the solution gives:

$$x(t) = \frac{1}{k}\left[1 - (1 + \omega_n t)e^{-\omega_n t}\right], \quad \omega_n = \sqrt{\frac{k}{m}}. \tag{38}$$

A.5.1 Derivation of $\tau^{(s)}$

The steady-state displacement is $x_\infty = \lim_{t\to\infty} x(t) = 1/k$. The velocity response is:

$$\dot{x}(t) = \frac{d}{dt}x(t) = \frac{1}{m}te^{-\omega_n t}. \tag{39}$$

From Definition 2.2:

$$\tau^{(s)} = \frac{1}{x_\infty}\int_0^\infty t\dot{x}(t)dt = k\int_0^\infty t \cdot \frac{1}{m}te^{-\omega_n t}dt = \frac{k}{m}\int_0^\infty t^2 e^{-\omega_n t}dt. \tag{40}$$

Using the standard integral formula for $a > 0$:

$$\int_0^\infty t^n e^{-at}dt = \frac{n!}{a^{n+1}}, \quad n = 0, 1, 2, \ldots \tag{41}$$

with $n = 2$ and $a = \omega_n$:

$$\int_0^\infty t^2 e^{-\omega_n t}dt = \frac{2}{\omega_n^3}. \tag{42}$$

Substituting (42) into (40) and noting $k/m = \omega_n^2$:

$$\tau^{(s)} = \omega_n^2 \cdot \frac{2}{\omega_n^3} = \frac{2}{\omega_n}. \tag{43}$$

A.5.2 Derivation of τ_{pole}

The Laplace transform of the velocity response (39) is:

$$\tilde{g}(s) = \mathcal{L}\{\dot{x}(t)\} = \frac{1}{m} \cdot \frac{1}{(s + \omega_n)^2}. \tag{44}$$

Evaluating at $s = 0$:

$$\tilde{g}(0) = \frac{1}{m\omega_n^2}, \tag{45}$$

$$\tilde{g}'(s) = -\frac{2}{m} \cdot \frac{1}{(s+\omega_n)^3}, \tag{46}$$

$$\tilde{g}'(0) = -\frac{2}{m\omega_n^3}. \tag{47}$$

From Definition 2.8:

$$\tau_{\text{pole}} = \left|\frac{\tilde{g}'(0)}{\tilde{g}(0)}\right| = \left|\frac{-2/(m\omega_n^3)}{1/(m\omega_n^2)}\right| = \left|-\frac{2}{\omega_n}\right| = \frac{2}{\omega_n}. \tag{48}$$

A.5.3 Equality Verification

Comparing (43) and (48):

$$\tau^{(s)} = \tau_{\text{pole}} = \frac{2}{\omega_n} = 0.6325 \text{ s}, \tag{49}$$

where the numerical value uses $\omega_n = \sqrt{1000/100} = \sqrt{10} \approx 3.1623$ rad/s. This completes the analytical verification of Theorem 3.3 for this critically damped LTI system.

A.5.4 Physical Interpretation

The equality $\tau^{(s)} = \tau_{\text{pole}} = 2/\omega_n$ has a clear physical interpretation:

- $\tau^{(s)}$ represents the temporal "center of mass" of the velocity response.
- τ_{pole} captures the spectral dominance of the double pole at $s = -\omega_n$.
- Both converge to $2/\omega_n$, which is exactly twice the time constant $1/\omega_n$ of a first-order system with the same natural frequency.

This derivation demonstrates that Theorem 3.3 provides a fundamental link between time-domain and frequency-domain characterizations of LTI system dynamics.

B Analytical Derivations for Theorem 3.4 Validation

B.1 CSTR (Single Exponential)

For $g(t) = \tau_0^{-1} e^{-t/\tau_0}$ with $\int_0^\infty g(t)dt = 1$:

$$\begin{aligned}
\tau_g^{(s)} &= \frac{1}{\tau_0}\int_0^\infty t e^{-t/\tau_0} dt = \tau_0, \\
\int_0^\infty g^2(t)dt &= \frac{1}{\tau_0^2}\int_0^\infty e^{-2t/\tau_0} dt = \frac{1}{2\tau_0}, \\
\tau^{(3)} &= \frac{1}{2\int_0^\infty g^2(t)dt} = \tau_0, \\
\rho_{13} &= \frac{\tau_g^{(s)}}{\tau^{(3)}} = 1.
\end{aligned}$$

B.2 PK Model (Bi-exponential)

For $g(t) = w_1\lambda_1 e^{-\lambda_1 t} + w_2\lambda_2 e^{-\lambda_2 t}$, normalized to unit area:

$$\begin{aligned}
\tau_g^{(s)} &= w_1/\lambda_1 + w_2/\lambda_2, \\
\int_0^\infty g^2(t)dt &= \frac{w_1^2\lambda_1}{2} + \frac{w_2^2\lambda_2}{2} + \frac{2w_1w_2\lambda_1\lambda_2}{\lambda_1+\lambda_2}, \\
\tau^{(3)} &= \frac{1}{2\int_0^\infty g^2(t)dt}, \\
\rho_{13} &= \frac{w_1/\lambda_1 + w_2/\lambda_2}{1/(2\int g^2)}.
\end{aligned}$$

Substituting the parameters from Table 5 yields $\rho_{13} = 3.0315$.

B.3 Sorption Model (Tri-exponential)

For $g(t) = \sum_{i=1}^3 w_i\lambda_i e^{-\lambda_i t}$:

$$\begin{aligned}
\tau_g^{(s)} &= \sum_{i=1}^3 \frac{w_i}{\lambda_i}, \\
\int_0^\infty g^2(t)dt &= \sum_{i=1}^3 \frac{w_i^2\lambda_i}{2} + \sum_{i<j} \frac{2w_iw_j\lambda_i\lambda_j}{\lambda_i+\lambda_j}, \\
\tau^{(3)} &= \frac{1}{2\int_0^\infty g^2(t)dt}, \\
\rho_{13} &= \frac{\sum w_i/\lambda_i}{1/(2\int g^2)}.
\end{aligned}$$

With the given parameters, $\rho_{13} = 26.3605$.

B.4 Proof of Impulse-Response Equivalence for $\tau^{(s)}$

Statement

For an LTI system with absolutely continuous step response $R(t)$ and impulse response $g(t)$ satisfying:

1. $g(t) = \dot{R}(t)$,
2. $R_\infty = \int_0^\infty g(t)\,dt = H \neq 0$,
3. $tg(t) \in L^1$ (finite first moment),

the signed centroid timescale equals the centroid of the impulse response:

$$\tau^{(s)} = \frac{1}{R_\infty}\int_0^\infty t\dot{R}(t)\,dt = \frac{1}{H}\int_0^\infty tg(t)\,dt = \tau_g^{(s)}.$$

Proof

By definition of the step response for an LTI system with zero initial conditions,

$$R(t) = \int_0^t g(\tau)\,d\tau.$$

Differentiating both sides yields

$$\dot{R}(t) = g(t).$$

The steady-state value is

$$R_\infty = \lim_{t\to\infty} R(t) = \int_0^\infty g(\tau)\,d\tau = H.$$

Substituting these relations into Definition 1:

$$\tau^{(s)} = \frac{1}{R_\infty}\int_0^\infty t\dot{R}(t)\,dt = \frac{1}{H}\int_0^\infty tg(t)\,dt = \tau_g^{(s)}.$$

The finiteness of the integral is guaranteed by the assumption $tg(t) \in L^1$. Thus, the two expressions are mathematically identical for any LTI system satisfying the integrability conditions.

Implications

1. This equivalence justifies the use of $\tau_g^{(s)}$ in Theorem 3.4 without loss of generality.
2. It provides two equivalent computational routes: one from step-response data ($R(t)$) and one from impulse-response data ($g(t)$).
3. For analytical derivations (as in Appendix B), the impulse-response form is often more convenient.

C Derivation of Theorem 3.6 for Mass–Spring–Damper System

Consider the underdamped step response

$$R(t) = 1 - \frac{e^{-\alpha t}}{\sqrt{1-\zeta^2}} \cos(\omega_d t - \phi), \quad \alpha = \zeta\omega_n,\ \omega_d = \omega_n\sqrt{1-\zeta^2},$$

with zero initial conditions.

The signed centroid is defined as

$$\tau^{(s)} = \frac{1}{R_\infty} \int_0^\infty t\dot{R}(t)\, dt.$$

Using integration by parts or Laplace transform, one obtains

$$\tau^{(s)} = \frac{\alpha}{\alpha^2 + \omega_d^2} = \frac{\zeta}{\omega_n}.$$

The unsigned centroid,

$$\tau^{(u)} = \frac{\int_0^\infty t|\dot{R}(t)|\, dt}{\int_0^\infty |\dot{R}(t)|\, dt},$$

is dominated by the exponential envelope for small ζ. The oscillatory component averages out, yielding

$$\tau^{(u)} \approx \frac{1}{\alpha} = \frac{1}{\zeta\omega_n}.$$

The envelope timescale $\tau_{\text{env}}^{(2)}$ is defined as the area under the envelope curve $e^{-\alpha t}$, giving $\tau_{\text{env}}^{(2)} = 1/\alpha$. The energy autocorrelation timescale $\tau_E^{(3)}$ follows from $E(t) \propto \dot{R}^2 + \omega_n^2 R^2 \sim e^{-2\alpha t}$, leading to $\tau_E^{(3)} = 1/(2\alpha)$.

Thus, the diagnostic ratios are:

$$\Delta_{su} = \frac{\tau^{(s)} - \tau^{(u)}}{\tau^{(u)}} = \frac{\zeta^2}{1} - 1 + \mathcal{O}(\zeta^4) = \zeta^2 - 1, \tag{50}$$

$$\Delta_{23}^{\text{env}} = \frac{\tau_{\text{env}}^{(2)} - \tau_E^{(3)}}{\tau_{\text{env}}^{(2)}} = \frac{1/\alpha - 1/(2\alpha)}{1/\alpha} = \frac{1}{2}. \tag{51}$$

These results hold asymptotically as $\zeta \to 0$, consistent with the weak-damping assumption of Theorem 3.6. **Note on the simplified response:** This derivation uses the approximate form $R(t) = 1 - e^{-\alpha t}\cos(\omega_d t)$, which omits the normalization factor $1/\sqrt{1-\zeta^2}$ and phase shift ϕ present in the exact response (Eq. 35). For the exact response, numerical integration yields $\tau^{(s)} \approx 2\zeta/\omega_n$ in the infinite-observation limit.